Green remediation of Cd and Hg contaminated soil using humic acid modified montmorillonite: immobilization performance under accelerated ageing conditions

Liuwei Wang[a], Xuanru Li[a], Daniel C.W. Tsang[b], Fei Jin[c], Deyi Hou[a*]

[a] School of Environment, Tsinghua University, Beijing 100084, China

[b] Department of Civil and Environmental Engineering, The Hong Kong Polytechnic University, Hung Hom, Kowloon, Hong Kong, China

[c] School of Engineering, University of Glasgow, Glasgow G12 8QQ, United Kingdom

*corresponding author (houdeyi@tsinghua.edu.cn)

Phone: +86-010-62781159

Abstract

Solidification/Stabilization (S/S) is an effective way to immobilize toxic metals in contaminated soil. However, utilization of ordinary Portland cement (PC) in this process has raised environmental concerns owing to the high carbon footprint from PC manufacturing and the risk of toxic element leaching in the long term. Hence there is an urgent need to seek for “green” immobilization approaches with long-term stability. In this study, a clay-based material, humic acid modified montmorillonite (HA-Mont) was applied to a Cd and Hg contaminated soil. Field emission scanning electron microscopy combined with energy-dispersive X-ray spectroscopy (FESEM/EDS), N_2 adsorption-desorption, Fourier transform infrared (FTIR) spectroscopy and X-ray diffraction (XRD) analyses were performed to investigate the characteristics of this material. Compared to the soil without any treatment, dosage of 5% HA-Mont could effectively reduce Cd and Hg concentrations by 94.1% and 93.0%, respectively and to below the regulatory limits in the TCLP (Toxicity Characteristic Leaching Procedure) leachates. Compared to the soil treated with virgin montmorillonite, HA modification resulted in the reduction of leachate concentrations of Cd and Hg by 69.5% and 65.9%, respectively. Long-term immobilization performance of the HA-Mont treatment was examined using a quantitative accelerated ageing method. In order to examine the ageing features, a novel method based on conditional probability was developed, and the reliability of HA-Mont immobilization was found to fit the Weibull model well, as the ageing rate of immobilization effect increased with time. After 120 years of ageing, reliability of both

metals could still remain above 0.95. Cd concentration in TCLP leachates at 120th year could still remain below the regulatory limit (294 μg/L vs 1000 μg/L), while Hg concentration reached the regulatory limit of 200 μg/L in 96th year. This is the first attempt developing a green S/S method of Cd and Hg contaminated soil using HA-Mont and examining the long-term ageing characteristics of the stabilized soil using a probability-based approach.

Keywords: clay minerals; metal immobilization; accelerated ageing; long-term leachability; probability-based approach.

1. Introduction

Soil contamination is a major environmental problem, posing risks to human health and ecosystems (Bampa et al. 2019; Duval et al. 2019; Ma et al. 2019; O'Connor et al. 2019; Wang et al. 2019b). In China, it is estimated that about 16.1% of soils contained toxic metals and organic contaminants exceeding soil quality standards (MEP 2014). Toxic elements in soil could cause severe health problems (Zhang et al. 2019). Among the contaminants, toxic metal(loid)s such as mercury (Hg), cadmium (Cd), lead (Pb), arsenic (As), and chromium (Cr) are of significant concerns owing to their severe effect to humans and other organisms. For instance, Hg is regarded as one of "ten leading chemicals of concern" by the World Health Organization (WHO 2017). It has been proven that mercuric cation, Hg^{2+}, can cause damage to kidney and lung, while the organomercuric form impairs brain function (Clarkson and Magos 2006). Cd can cause softening of the bones and kidney failure (i.e. Itai-itai disease) (Rizwan et al. 2018; Shen et al. 2019c). Remediation of soil Hg and Cd contamination can be achieved by conventional methods such as soil washing (Sierra et al. 2010), cement-based solidification/stabilization (S/S)(Shen et al. 2019a), containment (NJDEP 2014) and electrokinetic removal (Figueroa et al. 2016). However, with the emergence of "green and sustainable remediation" (GSR) movement, "greener" remediation methods are encouraged in order to assure the sustainability of the remediation process (Hou et al. 2016; Hou and Al-Tabbaa 2014; Krzywoszynska 2019; Song et al. 2019; Zhang et al. 2020). It is therefore imperative to explore remediation technologies with lower carbon footprint and higher net environmental benefit.

Solidification/stabilization is a cost-effective approach aiming at immobilizing toxic metals through physical encapsulation and chemical stabilization. Based on the types of amendments in this process, S/S can be divided into several categories such as cement-based S/S, lime-based S/S, thermoplastic method and polymerization method (Wang et al. 2012). Among these types, Portland cement (PC) is the most widely used owing to its universal applicability and low cost (Wang et al. 2018b). However, cement-based S/S aggravates carbon footprints. It is estimated that PC production accounts for 8% of global anthropogenic CO_2 emissions (0.66-0.82 t CO_2/t) (Shen et al. 2015). In addition, long-term stability of cement-based S/S is often overlooked (Jing et al. 2019; Shen et al. 2019a).

A variety of novel S/S agents have been investigated in recent years, such as biochar (O'Connor et al. 2018; Shen et al. 2019b), geopolymer (Dassekpo et al. 2018), layered double hydroxides (Hudcova et al. 2019), apatite (Markovic et al. 2019) and clay minerals (Chen et al. 2019). Clay minerals are plentiful in nature. Owing to the high specific surface area, excellent stability and tunable interlayer characteristics, clay minerals have been studied extensively as sorbents (Mukhopadhyay et al. 2019), and recent studies have examined the feasibility of using clay minerals as immobilizing agents in soil remediation processes. For instance, a study by Liang et al. (2019) used mercapto-modified attapulgite for the remediation of Cd contaminated alkaline agricultural soill. It has been found that addition of 0.2 wt. % modified attapulgite could effectively reduce Cd concentration in TCLP leachates by 16.3%, and surface complexation rather than liming was the fundamental stabilization

94 mechanism. Another study by Wang et al. (2019a) developed a clay-based S/S
95 method using metakaolin-lime mixture for As and Pb immobilization. Addition of 15wt. %
96 of mixture could successfully reduce leachate As and Pb concentrations by 96.2%
97 and 98.8%, respectively, owing to the enhanced hydration of clay induced by lime. In
98 general, mechanisms involved in clay-based S/S approaches may include surface
99 complexation (Liang et al. 2019), liming & precipitation (Wang et al. 2018a),
100 ion-exchange (Li et al. 2018) or induced encapsulation & fixation (Wang et al. 2019a),
101 depending on the type of clay (section 3.4) and modification strategies.
102 Montmorillonite $[(0.5Ca,Na)_{0.7}(Al,Mg,Fe)_4[(Si,Al)_8O_{20}](OH)_4 \cdot nH_2O]$ is a kind of 2:1 clay
103 mineral composed of two tetrahedral sheets of silica sandwiching a central octahedral
104 sheet of alumina (Rumble et al. 2018). It can adsorb metals effectively through ion
105 exchange in the interlayers of 2:1 sheet. However, raw montmorillonite has shown
106 poor stabilization performance, as the immobilized metals can be exchanged and
107 released in the long term (Brown et al. 2013). In order to improve the adsorption
108 capability of montmorillonite, various attempts have been made through inserting
109 functional groups and organic matters between the layers. Quaternary ammonium
110 cations (Bhattacharyya and Sen Gupta 2008), L-cystein (Mittal et al. 2016), humic
111 acid (Wu et al. 2011) as well as other agents have been used for montmorillonite
112 modification, but these studies solely investigated the adsorption performance in the
113 aqueous phase. Therefore, extending their utilization to metal-contaminated soil
114 stabilization may well serve as an effective approach in achieving GSR.
115 One critical issue in S/S processes is the long-term stability. Although short-term

116 immobilization has proven to be satisfactory in most cases, numerous environmental
117 factors will affect the stabilization performance in the long run. One method to
118 evaluate the temporal effect of immobilization approaches is to simulate real
119 occurrences of specific environmental stresses in laboratory via quantitative
120 accelerated ageing tests (Shen et al. 2018a). However, although the influence of
121 ageing on metal mobility was investigated, the ageing features (i.e. ageing rate and
122 stabilization reliability) were poorly understood. Therefore, a method to describe or
123 predict the ageing characteristics of stabilization processes is needed.
124 In this context, humic acid modified montmorillonite was selected as an immobilization
125 agent for a Cd and Hg contaminated agricultural soil. A novel method based on
126 conditional probability theory was developed to describe the ageing features of the
127 stabilization process. This study intends to: (1) reveal the effect of humic acid
128 modification on the interlayer characteristics of montmorillonite and its adsorption
129 performance; (2) quantitatively investigate the Hg and Cd stabilization efficiency in the
130 long term; (3) describe the ageing characteristics of the immobilization processes,
131 and validate the applicability of this novel material for long-term green stabilization.

132 # 2. Materials and methods

133 ## 2.1 Materials

134 Commercially available montmorillonite (hereinafter referred as Mont) was purchased
135 from Aladdin Company Co. Ltd. All chemicals (analytical grade) such as humic acid,
136 cadmium(II) nitrate tetrahydrate [$Cd(NO_3)_2 \cdot 4H_2O$], CH_3COOH, mercury(II) nitrate

monohydrate [$Hg(NO_3)_2 \cdot H_2O$], NaOH, HNO_3, $NaNO_3$ were purchased from Macklin Company Co. Ltd.

2.2 Synthesis of humic acid modified montmorillonite

Humic acid-modification was conducted in batch experiments. Humic acid of 0.5 g was dissolved in 1 L 0.1 M $NaNO_3$, with pH adjusted to 8.5 with HNO_3 and NaOH. Montmorillonite powders of 3 ± 0.001 g were added to 300 mL HA solution in a 500 mL conical flask (1:100 solid to liquid ratio). All the weightings were conducted on an electronic balance with a precision of 0.001 g. Mixtures were shaken in a thermostatic mechanical shaker (298 K, 170 r/min) for 24 h. The solid separation was then performed via centrifugation at 4000 r/min, and washed with deionized water. The solids (hereinafter referred as HA-Mont) were then air-dried in a fume hood to reach a constant weight (~24 h).

2.3 Batch adsorption experiments

The HA-Mont was subjected to sorption tests in aqueous solutions. Cd^{2+} and Hg^{2+} solutions were prepared separately using analytical grade $Cd(NO_3)_2 \cdot 4H_2O$ and $Hg(NO_3)_2 \cdot H_2O$ and deionized water. The influence of pH on Cd and Hg adsorption behavior was examined in a wide range of pH (i.e. 3-11). In the batch adsorption tests, HA-Mont of 0.1 g was added to 10 ± 0.01 mL (1:100 solid to liquid ratio) of 100 mg/L Cd^{2+} and Hg^{2+} solution for each sorption test. Mixtures were then shaken for 24 h at 298 K. Effects of initial Cd & Hg concentration and time were also examined in order

157 to study the adsorption isotherm and adsorption kinetics. The isotherm study was
158 conducted at different initial concentrations of Cd^{2+} and Hg^{2+} (i.e. 0.1, 0.5, 1, 10, 50,
159 100 mg/L, pH = 8.4 in accordance with soil pH) with a 1:100 solid to liquid ratio and
160 the equilibrium time was set as 24 h. The adsorption data was fitted by Freundlich
161 model (Eq. 1):

$$q_e = K c_e^{\frac{1}{n}} \qquad (1)$$

162 where q_e represents solid-phase metal ion concentration at equilibrium (mg/g), c_e
163 represents liquid-phase metal ion concentration at equilibrium (mg/L), while n and K
164 represent the Freundlich isotherm constant.
165 Influence of contact time (30 min, 60 min, 3 h, 10 h, 18 h and 24 h) was investigated at
166 initial concentrations of 100 mg/L Cd^{2+} and Hg^{2+} to infer the adsorption kinetics. At the
167 designated time intervals, the supernatant was separated from the mixture via
168 centrifugation (at 4000 r/min for 5 min) and then filtration with 0.45 μm membrane
169 syringe filter. Pseudo-second order model (Eq. 2) was used to describe the adsorption
170 kinetics of HA-Mont:

$$q_t = \frac{k_2 q_e^2 t}{1 + k_2 q_e t} \qquad (2)$$

171 where q_t and q_e (mg/g) represent solid-phase metal ion concentration at time t (min)
172 and equilibrium, respectively. k_2 ($g \cdot mg^{-1} \cdot min^{-1}$) is a constant.

173 2.4 Soil treatment

174 The soil was collected from an agricultural field (top 30 cm) in a suburban area of
175 Beijing. Soil properties are listed in Table 1. The soil was then air-dried in a fume hood,

ground and sieved to <2 mm. To examine the initial metal concentrations, the soil was digested in accordance with USEPA Method 1631 (USEPA 2001). The initial Cd and Hg concentrations were determined to be 0.08 and 0.025 mg/kg, respectively. The soil was then spiked to a contamination level of 100 mg/kg Hg and 100 mg/kg Cd as per O'Connor et al. (2018). Briefly, 1 L of 100 mg/L Cd^{2+}&Hg^{2+} solution was added to 1 kg virgin soil. The mixture was then thoroughly homogenized in a sealed bag, and put in a tray and air-dried for 7 days (0.4% final water content). Soil conductivity and pH were measured in a 1:20 soil:deionized water slurry (wt.:vol.). Particle size distribution of the soil was determined using a laser particle size analyzer (LS13320, Beckman Coulter Inc., US) in the dry mode. According to the United States Department of Agriculture Classification System, the texture of the soil was sandy loam. Total organic matter content of the soil was analyzed by a TOC analyzer (TOC-V, Shimadzu, Japan).

Table 1 Physiochemical properties of the soil used in this study.

Property	Value[a]
pH	8.44 ± 0.02
Electrical conductivity (μS/cm)	90.43 ± 0.29
Total organic matter content (%)	1.72 ± 0.03
Clay (<0.002 mm, %)	2.46 ± 0.01
Silt (0.002-0.05 mm, %)	34.25 ± 0.09
Sand (0.05-2 mm, %)	63.29 ± 0.10
Total Cd (mg/kg)[b]	0.08 ± 0.01
Total Hg (mg/kg)[b]	0.025 ± 0.002

[a] mean ± standard deviation, n=3.

[b] prior to spiking

Dosages of 1%, 2%, 5%, 8% Mont and HA-Mont were applied to the Cd & Hg

194 artificially co-contaminated soil, and homogenized in a sealed bag. Each sample was
195 incubated with 40 wt. % water content (water to dry soil) (O'Connor et al. 2018; Shen
196 et al. 2019b), including an untreated sample of contaminated soil. Both treated and
197 untreated samples were incubated at constant moisture at 298 K for 7 days, and dried
198 in a fume hood for a further 7 days to reach a constant weight (final moisture < 1.4
199 wt.%).

200 2.5 Leaching and ageing processes

201 In order to investigate the mobility of Cd and Hg after HA-Mont amendment, TCLP
202 (Toxicity Characteristic Leaching Procedure) leaching test (USEPA 1992) was
203 conducted. Diluted CH_3COONa solution (initial pH 4.93 ± 0.05) was selected as the
204 buffer solution, and the mixture was subjected to leaching for 18 h at 296 K with a
205 liquid to solid ratio of 20:1. Immediately after the leaching procedure, the supernatant
206 was separated through centrifugation (4000 r/min, 5 min) and filtration (0.45 μm).
207 Decrease in leachate metal concentrations (DLMC) of different dosages can be
208 calculated by Eq. 3:

$$\mathrm{DLMC}(\%) = \frac{c_0 - c}{c_0} \times 100\% \qquad (3)$$

209 Where c_0 refers to the leachate concentrations without HA-Mont addition, c
210 represents the leachate metal concentrations under different dosages.
211 A quantitative artificial ageing method was adapted from Shen et al. (2018a) to
212 simulate the effect of rainfall. In brief, CO_2 saturated water (pH=5.6) was prepared via
213 injecting CO_2 into deionized water at 0.3 MPa for 15 min. Assuming 1 m^3 of soil

receives 2000 mm rainfall annually, it can be calculated that 1 g dry soil receives 1.538 mL rain water in 1 year (bulk density 1.3 g/cm^3). In each wetting process, artificially prepared rain water was added to the soil sample at a solid to liquid ratio of 1:12.304, and shaken for 8 h at 75 r/min. According to the calculation, one wetting cycle simulates 8 years of rainfall's effect on the treated soil. The liquid was discarded after the wetting cycle, and the soil was then air-dried for approximately 24 h prior to the next wetting cycle. A total of 15 wetting-drying cycles were conducted.

2.6 Characterization

Inductively coupled plasma mass spectrometry (ICP-MS) (Thermo Fisher iCAP RQ) was used to measure Cd and Hg concentrations in the filtrates after dilution and acidification. Field emission scanning electron microscopy (FESEM) (GEMINISEM 500, ZEISS, Germany) (SE2 mode, 15 kV) was used to investigate the morphology of Mont and HA-Mont. The surface chemical compositions of Mont and HA-Mont was analyzed by energy-dispersive X-ray spectroscopy (EDS). Their specific surface areas were determined by N_2 adsorption-desorption at 77 K (Autosorb-1MP, Quantachrome, US) using the BET method. Mont and HA-Mont were degassed at 105 °C for 12 h. Pore volume and pore size were given by the DFT equation. Fourier transform infrared spectra (FTIR) of samples were recorded using the KBr pellet method, over the wavenumber range of 4000 cm^{-1} to 400 cm^{-1} with 4 cm^{-1} resolution (NICOLET 870, NICOLET, US). X-ray diffraction (XRD) analysis, operating at 40 kV and 40 mA from 3°-90° 2θ using a diffractometer (D/max-2500, Rigaku, Japan) with

CuKα radiation (λ=0.15406 nm), were also performed after sieving (<0.048 mm) of Mont and HA-Mont to examine the changes of interlayer spacing.

3. Results and discussion

3.1 Material characterization

3.1.1 FESEM and EDS analyses

The morphology of the virgin montmorillonite and HA-Mont were shown in Fig. 1. After modification, montmorillonite particles surfaces became much smoother and appeared to stick together while in the virgin sample, small platelets were observed and particles were disintegrated. As shown in Table S1, the major elements on the surface of montmorillonite were O, Si and Al. Al^{3+} was replaced by Mg^{2+} in some aluminum octahedral layers (Ni et al. 2018).

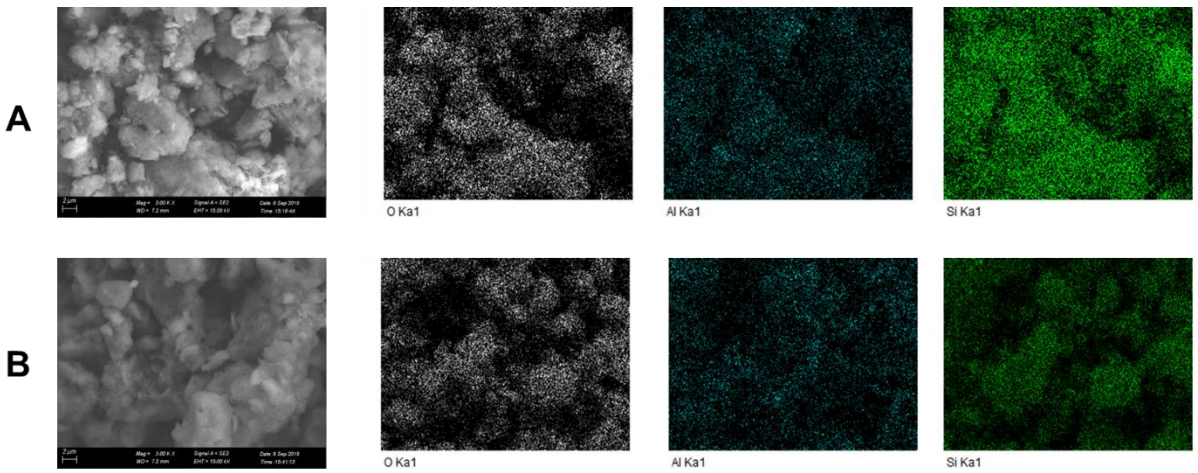

Fig. 1. Morphology and EDS scanning diagram of (A) montmorillonite and (B) humic acid modified montmorillonite.

250

251

252 3.1.2 BET analysis

253 The adsorption-desorption isotherms of montmorillonite and HA-Mont are presented
254 in Fig. S1. According to the International Union of Pure and Applied Chemistry (IUPAC)
255 classification system, the isotherms belong to Type IV isotherm, indicating
256 mesoporous structures of montmorillonite and HA-Mont. The hysteresis loop reveals
257 that at higher P/P_0, evaporation and capillary condensation took place, indicating
258 mesopores filling completion (Kuila and Prasad 2013). Specific surface area, average
259 pore diameter and pore volume were presented in Table 2. After modification, the BET
260 surface area decreased from 58.5 to 45.5 m^2/g. This is probably because the layer of
261 humic acid blocked the original pores in the interlayer of montmorillonite. A decrease
262 in pore diameter and pore volume confirmed this hypothesis. The BET results were
263 consistent with the FESEM observations, as the clay particles were covered by a
264 humic acid layer.

265

266

267

268

269 Table 2 Textural properties of montmorillonite and HA-Mont determined by nitrogen
270 adsorption-desorption.

Sample	Surface area (m^2/g)	Average pore diameter	Pore volume

		(nm)	(cm^3/g)
Mont	58.5	13.5	0.156
HA-Mont	45.5	9.91	0.113

271

272 ### 3.1.3 Adsorption study

273 Effect of initial solution pH on the adsorption efficiency is presented in Fig. 2, showing
274 better affinity of Cd(II) with HA-Mont than Hg(II). The maximum removal rates of Cd(II)
275 and Hg(II) were 97.6% and 83.9%, respectively. For Cd(II) adsorption, the removal
276 rate increased with the initial solution pH from 3 to 11. It is also noteworthy that
277 HA-Mont remains a high adsorption efficacy (>95%) across a wide range of initial
278 solution pH (i.e. 7-11). This is because the increase of OH^- concentrations increased
279 the negative charged sites on the interlayer surface of humic acid layer, resulting in an
280 increased adsorption efficacy (de Pablo et al. 2011). Under more acidic conditions, H^+
281 will cause competitive adsorption (i.e. preferential protonation), reducing the amount
282 of Cd(II) and Hg(II) sorbed to HA-Mont.

283

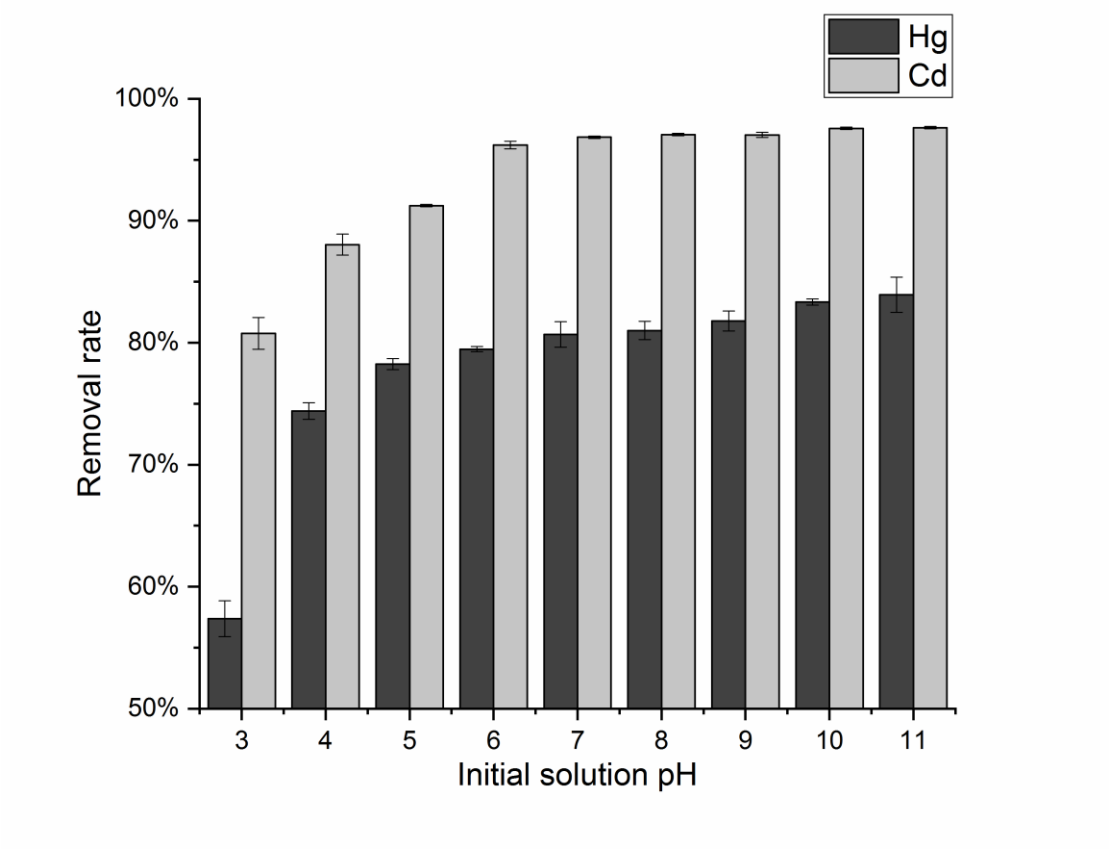

284

285 Fig. 2. Influence of initial solution pH on adsorption of Cd and Hg by HA-Mont.

286

287 Fig. 3(a) depicts the isothermal sorption characteristics of Cd(II) and Hg(II) at different
288 initial metal concentrations at 298 K. The derived parameters of Freundlich model are
289 presented in Table S2. The isotherm adsorption results indicate that both Cd(II) and
290 Hg(II) sorption to HA-Mont is nonideal adsorption on heterogeneous sites, which is
291 consistent with previous studies summarized in Table 3. Humic acid is a kind of
292 natural organic matter with various structures (Manahan 2017). As is presented in
293 Table 3, after modification by ligands with complicated structures, the surface of clay
294 minerals become more heterogeneous (adsorption tends to switch from monolayer
295 adsorption to multilayer adsorption). For instance, a study by Zauro and Vishalakshi
296 (2018) used pentin graft co-polymer montmorillonite composite for Cu^{2+}, Pb^{2+} and

297 Hg^{2+} adsorption. The isotherms were Freundlich-type owing to the complicated
298 structure of graft copolymer gel. As for the virgin montmorillonite, the adsorption
299 behavior mostly follows the Langmuir-type, owing to the homogeneity of the
300 interlayers between the 2:1 structures of this mineral (Liu et al. 2018; Stefan and
301 Stefan 2009; Wu et al. 2009).
302

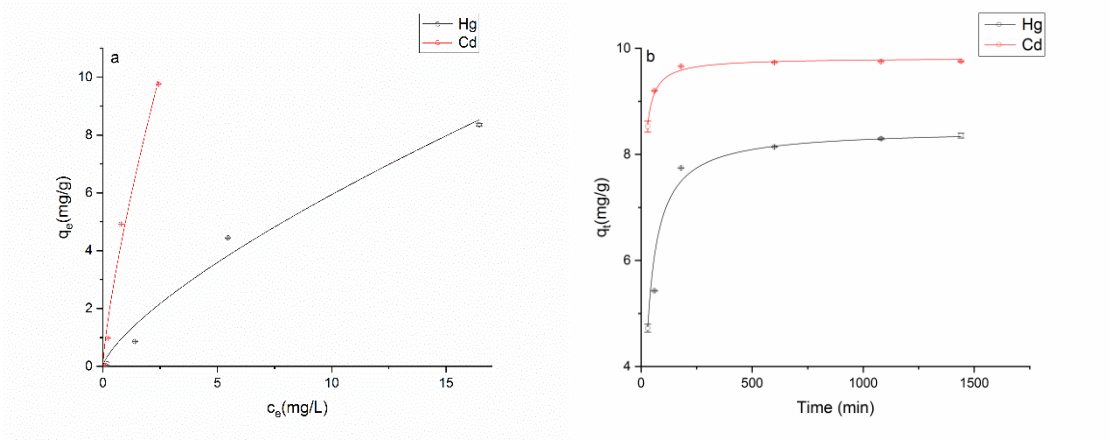

303
304 Fig. 3. (a) Cd and Hg adsorption isotherm of HA-Mont, and (b) Effect of time on Hg
305 and Cd adsorption (kinetics).
306
307 The effect of contact time on Cd(II) and Hg(II) adsorption is shown in Fig. 3(b). Owing
308 to the numerous adsorption sites of HA-Mont, adsorption of both metals increased
309 sharply initially. The adsorption rate decreased after 200 min and plateaued as the
310 number of available adsorption sites decreased. The derived parameters of this
311 model are presented in Table S3. A lower k_2 value was observed for Hg(II), indicating
312 that Hg(II) adsorption rate was slower than that of Cd(II). As shown in Table 3, most of
313 the studies involving Cd(II) and Hg(II) adsorption by minerals observed that
314 adsorption data can be best described by pseudo-second order model. This finding

315 indicates that in mineral-based sorption processes, the rate-limiting step tends to be

316 adsorption rather than diffusion (Shi et al. 2019).

317 Table 3 A comparison of Cd^{2+} and Hg^{2+} adsorption kinetics and isotherms by

318 mineral-based adsorbents.

Adsorbent	Metal ion	Optimum initial solution pH	Adsorption isotherm model	Adsorption kinetic model	Reference
Tripolyphosphate-modified kaolinite	Cd^{2+}	5.5	N.A.	Pseudo-second-order	(Adebowale et al. 2008)
Bentonite	Cd^{2+}	6-8	Freundlich	Pseudo-second-order	(Burham and Sayed 2016)
Ca-montmorillonite	Cd^{2+}, Hg^{2+}	4.8	Langmuir	Pseudo-second-order	(de Pablo et al. 2011)
Bentonite	Cd^{2+}	3	Langmuir	N.A.	(Karapinar and Donat 2009)
Amphoteric surfactant activated montmorillonite	Cd^{2+}	>7	Freundlich	Pseudo-second-order	(Liu et al. 2016)
Na-montmorillonite	Cd^{2+}	7	Langmuir	Pseudo-second-order	(Liu et al. 2018)
Vermiculite	Cd^{2+}	5	Langmuir	Pseudo-second-order	(Liu et al. 2010)
Zeolite	Cd^{2+}	>4	Freundlich	N.A.	(Merrikhpour and Jalali 2013)
Polyamide magnetic palygorskite	Hg^{2+}	N.A.	Langmuir	Pseudo-second-order	(Saleh et al. 2018)
Zeolite	Cd^{2+}	>7	Freundlich	Pseudo-second-order	(Shaban and Abukhadra 2017)
Hexadecyltrimethylammonium bromide modified clinoptilolite	Hg^{2+}	6-10	Langmuir	Pseudo-second-order	(Shirzadi and Nezamzadeh-Ejhieh 2017)
Na-montmorillonite	Cd^{2+}	>6.5	Langmuir	N.A.	(Stefan and Stefan 2009)
Mercaptoethylamine/Mercaptopropyltrimethoxysilane functionalized vermiculite	Hg^{2+}	7	Langmuir	Pseudo-second-order	(Tran et al. 2015)
Goethite–humic acid-modified kaolinite	Cd^{2+}	9	N.A.	Elovich	(Unuabonah et al. 2016)
Fe-montmorillonite	Cd^{2+}	>7	Langmuir	Pseudo-second-order	(Wu et al. 2009)
Pectin graft copolymer-montmorillonite	Hg^{2+}	9-13	Freundlich	Pseudo-second-order	(Zauro and Vishalakshi 2018)
Humic acid-montmorillonite complex	Cd^{2+}, Hg^{2+}	7-11	Freundlich	Pseudo-second-order	Present study

319

320 ### 3.1.4 FTIR spectra

321 Fig. 4 presents the FTIR spectra of humic acid solid and the adsorbents before and

322 after the batch adsorption test. The humic acid contains various oxygen-containing

323 functional groups such as hydroxyl, carbonyl and ester. As for the virgin clay and
324 modified sorbent, the wide band at wavenumber 3627 cm^{-1} represents the stretching
325 vibration of structural Al-OH groups in the octahedral structure of Mont and HA-Mont
326 (Long et al. 2013; Wu et al. 2011). The wide band appeared at 3433-3452 cm^{-1}
327 reveals the stretching vibrations of water (Skoog 2018). After humic acid modification
328 and metal adsorption, this absorption band shifted to higher wavenumber. This is
329 because humic acid decreased the interlayer spacing, thus decreasing the interlayer
330 water content (Skoog 2018; Wu et al. 2011). The 1639 cm^{-1} peak represents the
331 bending vibration of H_2O. The strong absorption peak around 1039-1043 cm^{-1} was
332 because of the stretching vibrations of Si-O tetrahedral sheet, and peak at 1082 cm^{-1}
333 was attributed to stretching vibrations of Si-O amorphous silica (Madejova 2003). The
334 peak at 916 cm^{-1} was attributed to bending vibrations of Al_2OH (Madejova 2003), and
335 the peaks at 521 cm^{-1} and 463-469 cm^{-1} represent Si-O-Mg and Si-O-Fe vibrations,
336 respectively (Ni et al. 2018). After modification, the 3627 cm^{-1}, 1082 cm^{-1} and 1039
337 cm^{-1} bands remained, indicating that the intrinsic 2:1 lamellar structure of
338 montmorillonite was not damaged. Owing to ion exchange between Na^+/Ca^+ and
339 Cd^{2+}/Hg^{2+}, several absorption peaks related to interlayer H_2O shifted (Wu et al. 2011).
340 As can be seen, intensity of hydroxyl increased slightly after humic acid modification.
341 However, as signals of montmorillonite Si-O and humic acid C-O are overlapped, it is
342 hard to distinguish between Si-O and C-O groups of HA-Mont.
343

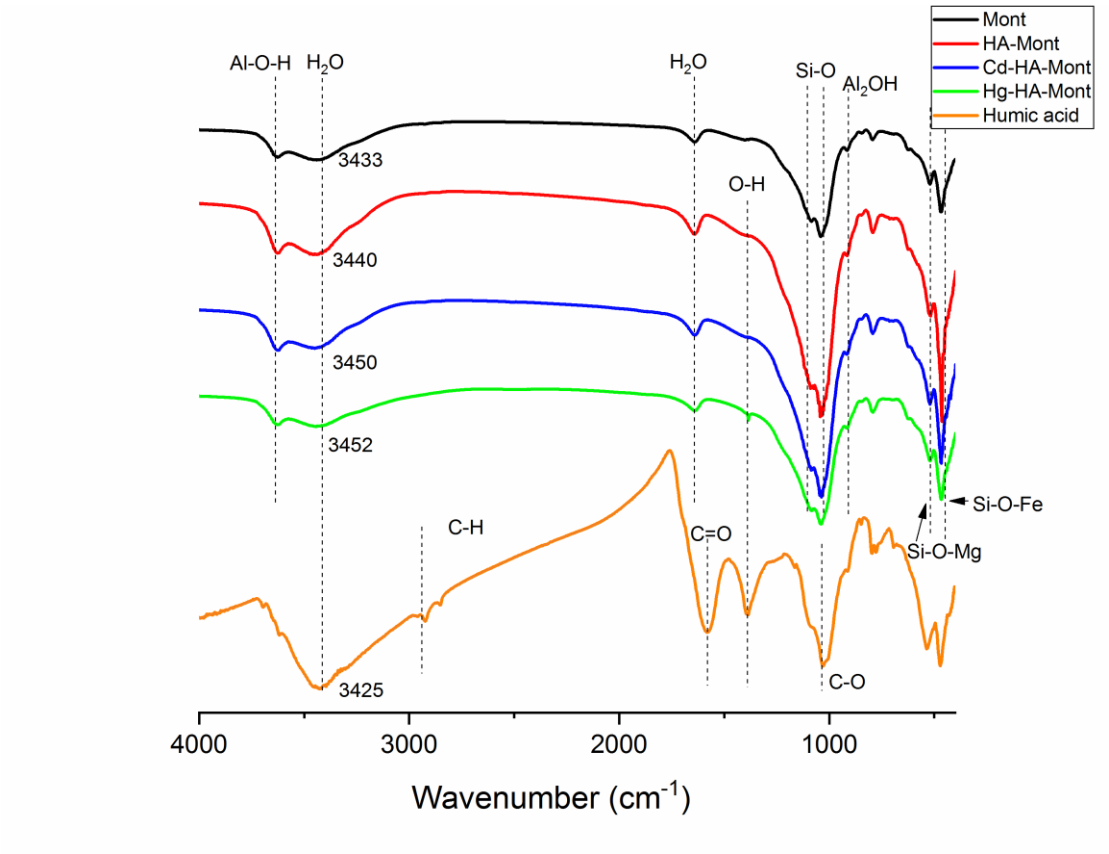

Fig. 4. FTIR spectra of Mont, HA-Mont, HA-Mont after 100 mg/L Cd^{2+} adsorption, HA-Mont after 100 mg/L Hg^{2+} adsorption, and humic acid.

3.1.5 XRD analysis

The XRD tests were performed before and after humic acid modification and metal adsorption to investigate the changes of interlayer spacing of montmorillonite. The interlayer spacing was calculated following the Prague equation (Zolotoyabko 2014)(Eq. 4):

$$2d\sin\theta = n\lambda \qquad (4)$$

Where d represents the interlayer spacing, λ represents the wavelength of X-ray, θ represents the glancing angle, and n is a positive integer. In this case, the 001 peak was used (n=1).

As is shown in Fig. 5, the basal spacing of the virgin montmorillonite was determined to be 1.528 nm. The 001 characteristic peak shifted slightly to the right after humic acid modification, indicating a smaller interlayer distance due to the adsorption of humic acid on the interlayer of montmorillonite. In addition, as the number of hydrophobic functional groups increased, the water content between the layers decreased, leading to a decreased spacing (Ni et al. 2018). It is also noteworthy that after modification, the intensity of 001 peak decreased. This is probably because the surface became more heterogeneous as the crystalline structure decreased (Guinebretiere 2007). In addition, peak broadening was observed after modification, indicating the crystal size became larger owing to humic acid adsorption (Skoog 2018).

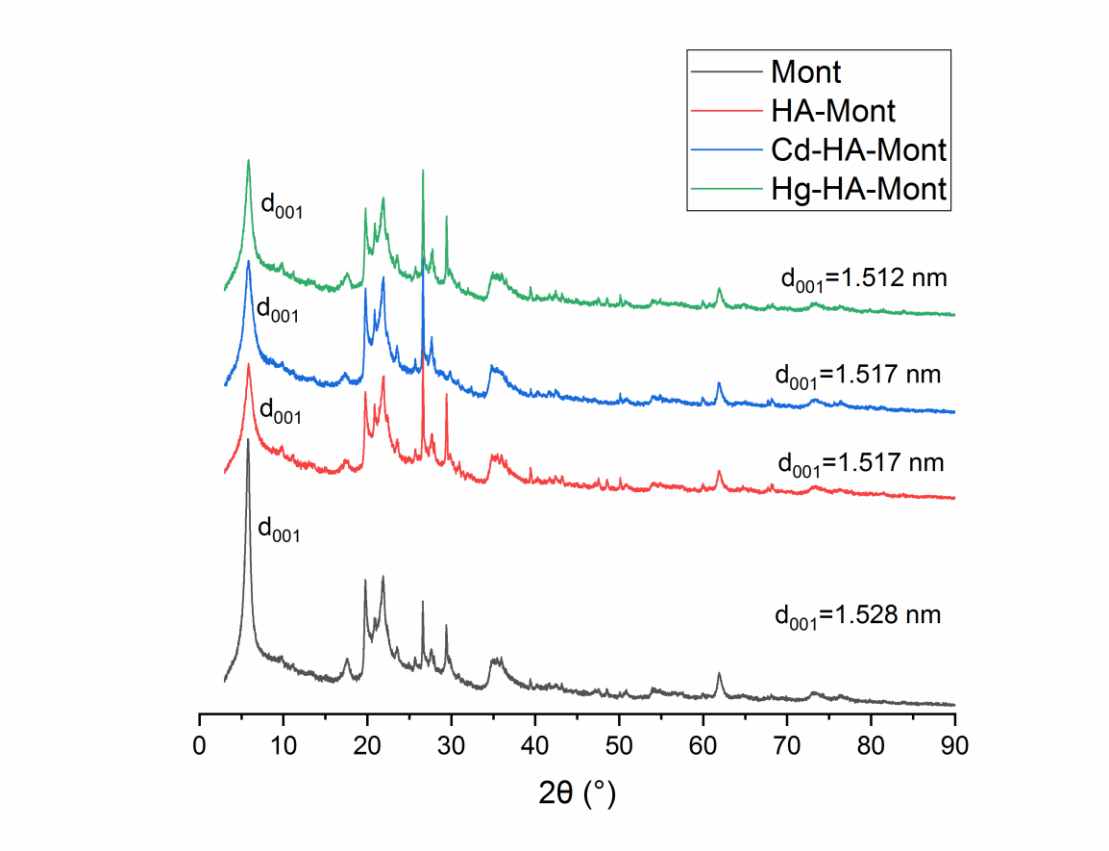

Fig. 5. X-ray diffractograms of Mont, HA-Mont, HA-Mont after 100 mg/L Cd^{2+}

adsorption and HA-Mont after 100 mg/L Hg^{2+} adsorption.

3.2 TCLP soil leaching

Cd and Hg concentrations in TCLP leachates are presented in Fig. 6. A higher dosage of amendments results in lower leachate concentrations of both metals. Addition of the virgin montmorillonite decreased the TCLP concentrations of Cd and Hg, but the immobilization effect was much weaker compared to that of HA-Mont. After humic acid modification, the leachate concentrations of Cd and Hg reduced by 69.5% and 65.9%, respectively, compared to that of virgin montmorillonite (at a dosage 5 wt.%). This is because the immobilization mechanism of virgin montmorillonite was mainly cation exchange and physisorption (Giese 2002; Yang et al. 2017). After humic acid modification, Cd and Hg could bind to more sites such as amine, hydroxyl, carboxyl and carbonyl through complexation, and the aromatic rings of humic acid promoted the cation-π interactions. As is shown in Fig. 6, an optimum dosage of 5 wt.% HA-Mont could immobilize both metals effectively, and the leachate concentrations of both metals were below the TCLP regulatory limits for non-hazardous wastes.

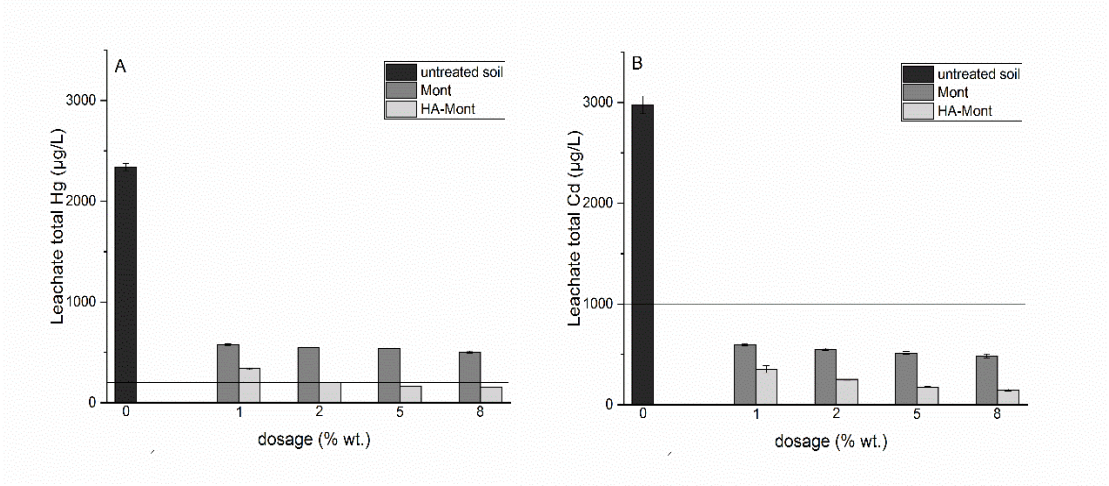

Fig. 6. TCLP leaching results: (A) leachate Hg concentrations and the TCLP non-hazardous regulatory limit for Hg (200 μg/L), (B) leachate Cd concentrations and the TCLP non-hazardous regulatory limit for Cd (1000 μg/L). Detection limit: 0.04 μg/L for Cd; 0.02 μg/L for Hg.

As shown in Fig. 6 and Fig. 7, although a dosage of 8% could reach a higher DLMC, the addition of 5% HA-Mont can effectively reduce the leachate Cd and Hg concentrations to below the TCLP non-hazardous regulatory limits. For both amendments, DLMC of Cd is higher than that of Hg under different dosages. This could be due to that the electronegativity of Cd is lower than that of Hg (1.7 vs 1.9). When metal ions form coordinate bonds, the difference in electron negativity of Cd and electron donors (i.e. O and N) were greater, indicating that the bond polarity of Cd complexes are higher (Weller 2018).

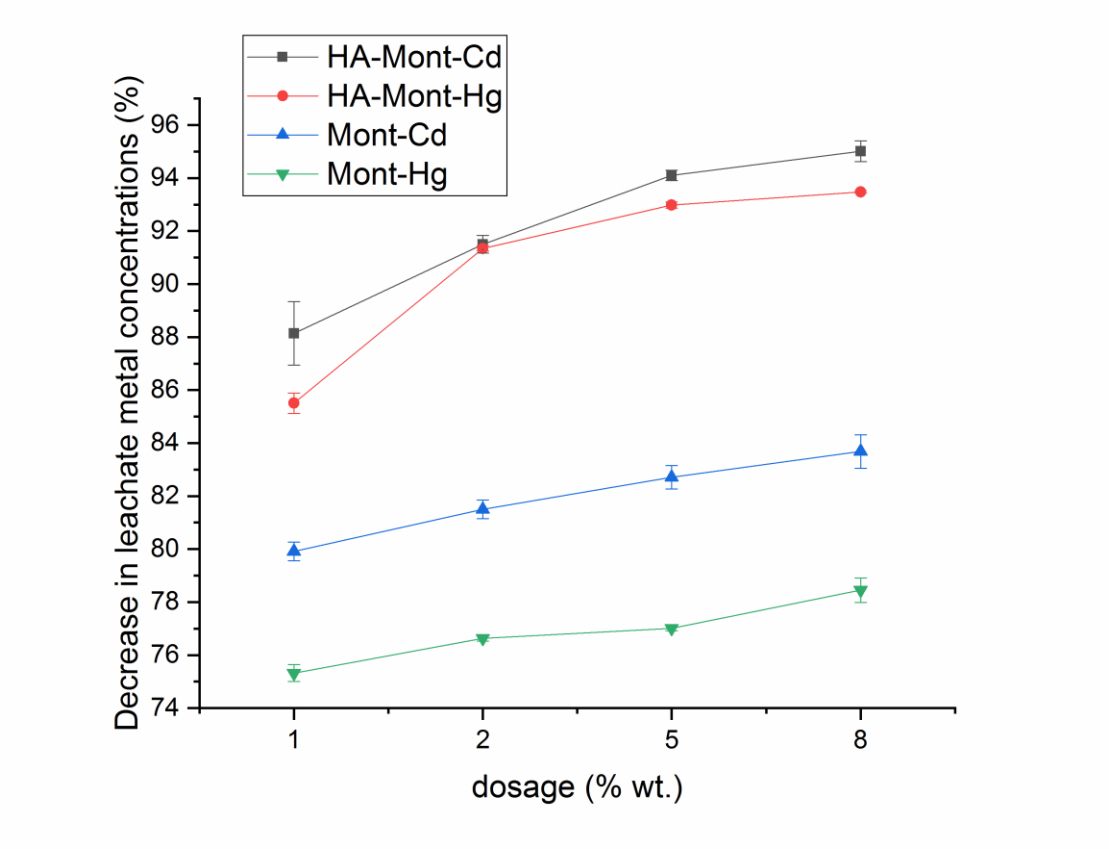

398

399 Fig. 7 Enhancement of Cd and Hg immobilization by amendment of montmorillonite or

400 HA-Mont.

401

402 3.3 Accelerated ageing

403 A total of 15 wetting-drying cycles were conducted to simulate 120 years of ageing

404 after HA-Mont assisted soil stabilization. TCLP leaching was conducted after each

405 drying cycle, and the leachate metal concentrations are presented in Fig. 8, showing a

406 monotone increasing trend with simulated time. After 120 years, leachate Cd

407 concentrations could still remain below the TCLP regulatory limit. In the 96th year,

408 leachate Hg concentration just reached the regulatory level of 200 μg/L. The results

409 indicate that HA-Mont is promising in stabilizing both metals.

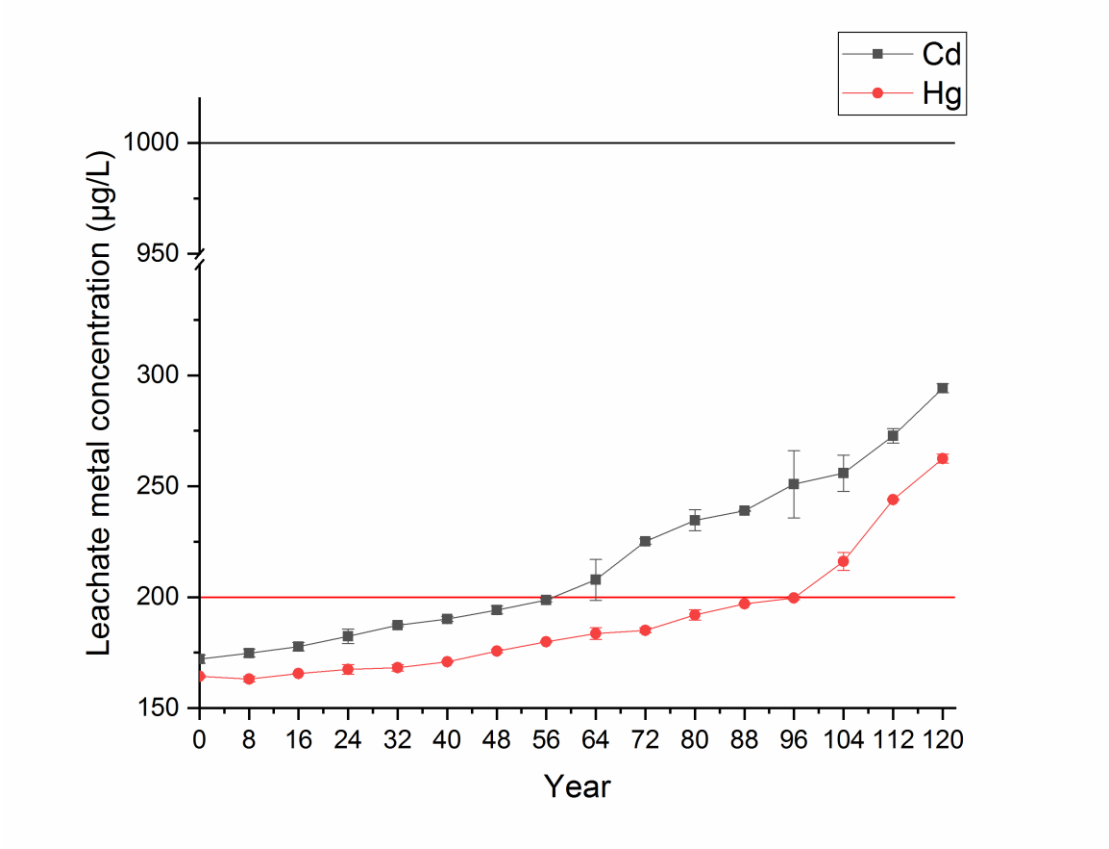

410

411 Fig. 8. Leachate metal concentrations under 120 years of accelerated ageing. The red
412 line represents the TCLP regulatory limit for Hg (200 μg/L), while the black line
413 represents the TCLP regulatory limit for Cd (1000 μg/L).

414

415 Although several studies have utilized accelerated ageing to examine the stabilization
416 performance of amendments, the ageing features were poorly investigated. Thus we
417 put forward a new method to investigate the long-term effectiveness of the
418 immobilization process. Metal immobilization can be simplified as the binding between
419 metals and certain functional sites. Assuming that at the beginning of the ageing
420 process (0^{th} year), the reliability of binding is 1 (all of the bindings were effective). With
421 ageing, owing to the complicated environmental stresses such as rainfall (Shen et al.
422 2018b), oxidation (Sheng et al. 2019) and freeze-thaw action (Hafsteinsdottir et al.

2011), some of the bindings are destabilitzed and thus decreasing the immobilization effect. This process can be described using the conditional probability theory:

$$\lim_{h\to 0}\frac{\mathrm{P}(\mathrm{t}\le \mathrm{T}\le \mathrm{t}+\mathrm{h})|\mathrm{T}>t)}{\mathrm{h}}=\lambda \qquad (5)$$

In Eq. 5, a binding at time t works effectively, until it breaks at time t+h. Thus λ refers to the ageing rate during the time interval of h. According to the probability theory, if the ageing rate is a constant λ_0 (the ageing of immobilization is not relevant to time), this process can be described using an exponential model. Its reliability [R(t)] can be described as follows:

$$\mathrm{R}(\mathrm{t})=e^{-\lambda_0 t} \qquad (6)$$

However, under field conditions, the ageing rate cannot be a constant. This process can better be depicted using the Weibull distribution (Rosin and Rammler 1933):

$$\lim_{h\to 0}\frac{\mathrm{P}(\mathrm{t}\le \mathrm{T}\le \mathrm{t}+\mathrm{h})|\mathrm{T}>t)}{\mathrm{h}}=\lambda(\mathrm{t})=\lambda_0 t^m \qquad (\mathrm{m}>1) \qquad (7)$$

If m=1, this model can be simplified as an exponential model.

The reliability function can be described as follows:

$$\mathrm{R}(\mathrm{t})=e^{-\lambda_0 t^{m+1}}=\ e^{-\lambda_0 t^{\alpha}} \qquad (8)$$

The reliability of HA-Mont immobilization under 120 years of accelerated ageing is presented in Fig. 9. Compared to the exponential model (Adj. r^2=0.953 and 0.811 for Cd and Hg, respectively), the Weibull model could better describe the ageing features of this process (Adj. r^2=0.984 and 0.979 for Cd and Hg, respectively), which reveals the increased distortion rate of the immobilization effect with time.

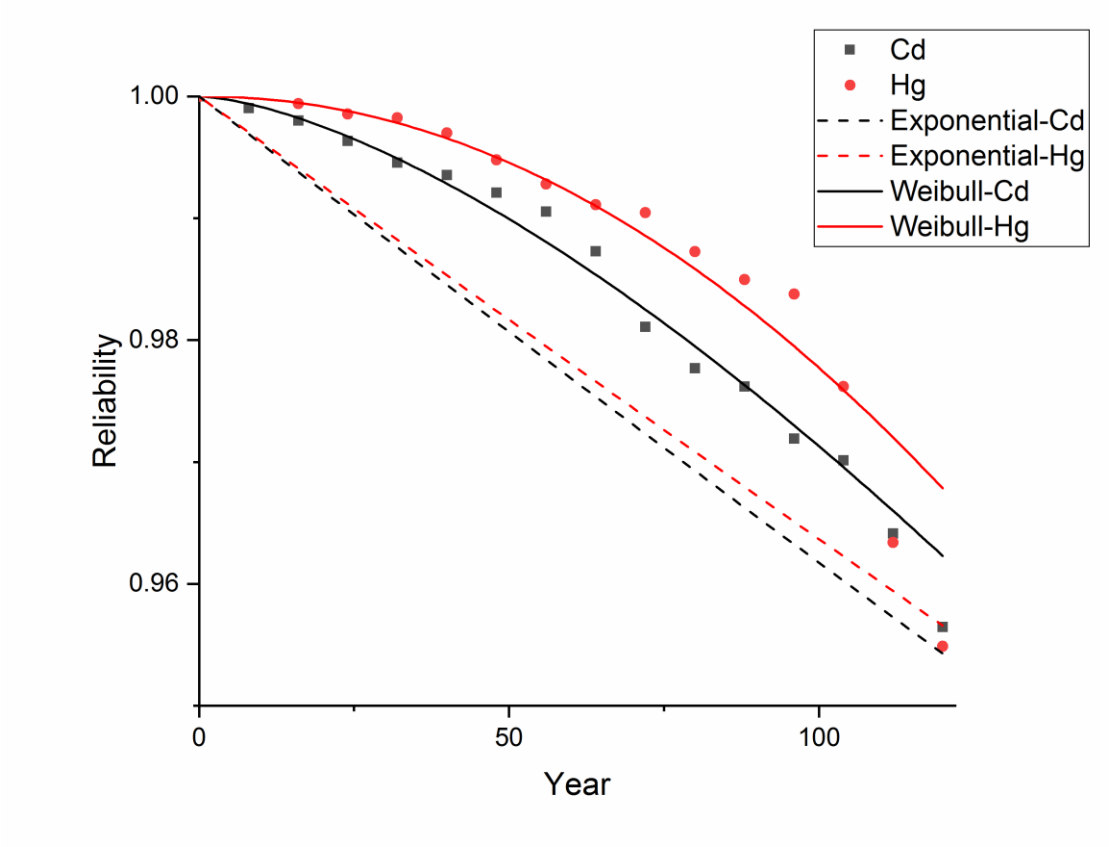

439

440 Fig. 9. Reliability of Cd and Hg immobilization under 120 years of accelerated ageing.

441

442 The value of α for Cd and Hg were 1.53 and 2.05, respectively, indicating that the
443 ageing rate λ for Cd increases much slower than that of Hg. After 120 years of
444 ageing, reliability of both metals could still remain above 0.95, demonstrating the
445 excellent long-term immobilization performance of HA-Mont.

446 ## 3.4 Discussion

447 According to the arrangement of silica and alumina sheets in the crystal structure,
448 clay minerals can be broadly divided into 1:1 and 2:1 types. A variety of clay minerals,
449 such as sepiolite (2:1), palygorskite (2:1), kaolinite (1:1), montmorillonite (2:1) and
450 vermiculite (2:1) have been applied for metal stabilization (Xu et al. 2017). It is

noteworthy that most of the clay-based adsorbents were 2:1 type. This is probably because 2:1 type clay minerals possess a higher surface area, higher ion exchange capacity as well as wider interlayer spacing, compared to 1:1 clay minerals (Bailey 1966; Chen et al. 2019). For instance, the strong hydrogen bond between the surface hydroxyl and oxygen atom of kaolinite, a typical 1:1 clay mineral, restricts its cation exchange capacity (only 3-15 cmol/kg). Besides, d_{001} of kaolinite was only 0.7 nm, making it impossible to contain cations between layers. These characteristics lead to a relatively low surface area. Compared to kaolinite, montmorillonite possesses a higher specific surface area, and adsorbate can not only sorb onto the outer surface but also the interlayers. The dominant force between two sandwich layers is van der Walls force, which is weaker than hydrogen bond, making it possible for ion exchange within the interlayers. In this study, an increase in interlayer spacing was observed after HA modification, and the weak force made the modification process much easier. Several mechanisms are involved in clay-based metal stabilization process, of which ion exchange plays a vital role. For instance, montmorillonite 2:1 sheet is negatively charged owing to the substitution of silicon by aluminum in the tetrahedral layer, and substitution of aluminum by magnesium in the octahedral layer, favoring sorption of metal ions between the sandwich layers for charge balance (Wu et al. 2011). In addition, surface hydroxyl groups of clay minerals (i.e. Al-O-H, Fig. 4) also promote adsorption through complexation (Xu et al. 2017).

However, natural clay minerals usually possess poor stabilization capability and suffer from a rapid diminishing of the immobilization effect with ageing. For instance, a study

473 by Wu et al. (2016) used sepiolite for Cd and Pb immobilization in a paddy soil. It was
474 found that the effect on exchangeable Pb decreased in 3 years. In light of these,
475 humic acid was selected in the present study to improve the immobilization
476 performance as well as the long-term effectiveness of clay mineral-based soil
477 stabilization process. Humic acid was a kind of natural organic matter, which
478 possesses a variety of nitrogen and oxygen-containing functional groups, including
479 hydroxyl, carbonyl, carboxyl, cyan, amide and ester (Manahan 2017). The
480 complexation between metals and these functional groups can greatly improve the
481 long-term effectiveness of metal immobilization (Lwin et al. 2018; Xu et al. 2017). In
482 addition, Cπ-cation interactions between metals and aromatic rings of humic acid also
483 promoted adsorption (Tran et al. 2017; Xia et al. 2019). The results from the present
484 study clearly showed that humic acid modification of montmorillonite promoted both
485 the short-term and long-term immobilization performance of Cd and Hg in a soil,
486 which could be ascribed to the mechanisms mentioned above. Although unmodified
487 montmorillonite could immobilize both metals through ion exchange, physisorption
488 and surface complexation (with structural hydroxyl groups), humic acid could
489 significantly promote the immobilization performance, since the surface complexation
490 was enhanced by oxygen-containing functional groups provided by humic acid.
491 It is of note that in field conditions, more parameters contribute to the ageing process.
492 Apart from rainfall, other environmental factors such as freeze-thaw cycles,
493 groundwater flow, and microbial activity may also affect the long-term effectiveness of
494 stabilization processes. Therefore, the artificial ageing method is suggested to take

more environmental factors into account, in order to perform a better prediction. Besides, if long-term monitoring data of a certain S/S treated field can be acquired, it may be helpful to judge whether an accelerated ageing method is suitable as compared with data from the field.

4. Conclusions

A green immobilization amendment, humic acid modified montmorillonite, was synthesized and used for Cd and Hg stabilization in soil. FESEM, EDS, BET, FTIR and XRD results reveal that humic acid was introduced to the interlayer of montmorillonite successfully. The adsorption behavior of both metals was well-fitted by Freundlich isotherm model and pseudo-second order kinetics model. When applying HA-Mont to a spiked Cd & Hg co-contaminated agricultural soil (100 mg/kg Cd and 100 mg/kg Hg), both metals could be effectively stabilized. A dosage of 5% HA-Mont could effectively reduce the leachate metal concentrations below the TCLP non-hazardous criteria for both metals. Compared to the virgin montmorillonite, a dosage of 5% HA-Mont could effectively reduce the leachate Cd and Hg concentrations by 69.5% and 65.9%, respectively and both below the TCLP regulatory limits for non-hazardous wastes. A novel approach using the conditional probability theory to describe the ageing characteristics of the treated soil was proposed. The Weibull model was found to describe the ageing characteristics well using the simulated ageing tests due to rainfall actions. HA-Mont could immobilize both metals effectively in the long term, since the reliability of both metals remained

above 0.95 after the simulated 120 years of ageing. It was suggested that future research should examine the stabilization performance of HA-Mont at the field scale and also compare and link artificial ageing results with available field ageing data.

Acknowledgements

This work was supported by the National Key Research and Development Program of China (Grant No. 2018YFC1801300).

References

Adebowale, K.O.; Unuabonah, E.I.; Olu-Owolabi, B.I. Kinetic and thermodynamic aspects of the adsorption of Pb^{2+} and Cd^{2+} ions on tripolyphosphate-modified kaolinite clay. Chem. Eng. J. 2008;136:99-107

Bailey, S.W. Clays and clay minerals : proceedings. Oxford : Pergamon Press; 1966

Bampa, F.; O'Sullivan, L.; Madena, K.; Sandén, T.; Spiegel, H.; Henriksen, C.B.; Ghaley, B.B.; Jones, A.; Staes, J.; Sturel, S.; Trajanov, A.; Creamer, R.E.; Debeljak, M. Harvesting European knowledge on soil functions and land management using multi-criteria decision analysis. Soil Use Manage. 2019;35:6-20

Bhattacharyya, K.G.; Sen Gupta, S. Adsorption of a few heavy metals on natural and modified kaolinite and montmorillonite: A review. Adv. Colloid Interface Sci. 2008;140:114-131

Brown, L.; Seaton, K.; Mohseni, R.; Vasiliev, A. Immobilization of heavy metals on

536 pillared montmorillonite with a grafted chelate ligand. J. Hazard. Mater.
537 2013;261:181-187
538 Burham, N.; Sayed, M. Adsorption Behavior of Cd^{2+} and Zn^{2+} onto Natural Egyptian
539 Bentonitic Clay. Minerals 2016;6:15
540 Chen, G.; Shah, K.J.; Shi, L.; Chiang, P.-C.; You, Z. Red soil amelioration and heavy
541 metal immobilization by a multi-element mineral amendment: Performance
542 and mechanisms. Environ. Pollut. 2019;254:112964
543 Clarkson, T.W.; Magos, L. The toxicology of mercury and its chemical compounds.
544 Crit. Rev. Toxicol. 2006;36:609-662
545 Dassekpo, J.B.M.; Ning, J.Q.; Zha, X.X. Potential solidification/stabilization of
546 clay-waste using green geopolymer remediation technologies. Process Saf.
547 Environ. Protect. 2018;117:684-693
548 de Pablo, L.; Chavez, M.L.; Abatal, M. Adsorption of heavy metals in acid to alkaline
549 environments by montmorillonite and Ca-montmorillonite. Chem. Eng. J.
550 2011;171:1276-1286
551 Duval, M.E.; Martinez, J.M.; Galantini, J.A. Assessing soil quality indices based on
552 soil organic carbon fractions in different long-term wheat systems under
553 semiarid conditions. Soil Use Manage. 2019;
554 Figueroa, A.; Cameselle, C.; Gouveia, S.; Hansen, H.K. Electrokinetic treatment of an
555 agricultural soil contaminated with heavy metals. J. Environ. Sci. Health Part A
556 Toxic Hazard. Subst. Environ. Eng. 2016;51:691-700
557 Giese, R.F. Colloid and surface properties of clays and related minerals. New York.

558 New York : Marcel Dekker, Inc.; 2002
559 Guinebretiere, R. X-ray diffraction by polycrystalline materials. London Newport
560 Beach, CA : ISTE; 2007
561 Hafsteinsdottir, E.G.; White, D.A.; Gore, D.B.; Stark, S.C. Products and stability of
562 phosphate reactions with lead under freeze-thaw cycling in simple systems.
563 Environ. Pollut. 2011;159:3496-3503
564 Hou, D.; Guthrie, P.; Rigby, M. Assessing the trend in sustainable remediation: A
565 questionnaire survey of remediation professionals in various countries. J.
566 Environ. Manage. 2016;184:18-26
567 Hou, D.Y.; Al-Tabbaa, A. Sustainability: A new imperative in contaminated land
568 remediation. Environ. Sci. Policy 2014;39:25-34
569 Hudcova, B.; Vitkova, M.; Ourednicek, P.; Komarek, M. Stability and stabilizing
570 efficiency of Mg-Fe layered double hydroxides and mixed oxides in aqueous
571 solutions and soils with elevated As(V), Pb (II) and Zn(II) contents. Sci. Total
572 Environ. 2019;648:1511-1519
573 Jing, J.; Christensen, J.T.; Sørensen, P.; Christensen, B.T.; Rubæk, G.H. Long-term
574 effects of animal manure and mineral fertilizers on phosphorus availability and
575 silage maize growth. Soil Use Manage. 2019;35:323-333
576 Karapinar, N.; Donat, R. Adsorption behaviour of Cu^{2+} and Cd^{2+} onto natural bentonite.
577 Desalination 2009;249:123-129
578 Krzywoszynska, A. Making knowledge and meaning in communities of practice: What
579 role may science play? The case of sustainable soil management in England.

580 Soil Use Manage. 2019;35:160-168
581 Kuila, U.; Prasad, M. Specific surface area and pore-size distribution in clays and
582 shales. Geophys. Prospect. 2013;61:341-362
583 Li, S.S.; Wang, M.; Zhao, Z.Q.; Ma, C.B.; Chen, S.B. Adsorption and Desorption of Cd
584 by Soil Amendment: Mechanisms and Environmental Implications in Field-Soil
585 Remediation. Sustainability 2018;10:14
586 Liang, X.F.; Li, N.; He, L.Z.; Xu, Y.M.; Huang, Q.Q.; Xie, Z.L.; Yang, F. Inhibition of Cd
587 accumulation in winter wheat (Triticum aestivum L.) grown in alkaline soil
588 using mercapto-modified attapulgite. Sci. Total Environ. 2019;688:818-826
589 Liu, C.M.; Wu, P.X.; Zhu, Y.J.; Tran, L.T. Simultaneous adsorption of Cd^{2+} and BPA on
590 amphoteric surfactant activated montmorillonite. Chemosphere
591 2016;144:1026-1032
592 Liu, W.; Zhao, C.C.; Wang, S.T.; Niu, L.; Wang, Y.L.; Liang, S.X.; Cui, Z. Adsorption of
593 cadmium ions from aqueous solutions using nano-montmorillonite: kinetics,
594 isotherm and mechanism evaluations. Res. Chem. Intermed.
595 2018;44:1441-1458
596 Liu, Y.; Li, H.; Zhu, X.H. Competitive Adsorption of Ag^{+}, Pb^{2+}, Ni^{2+}, and Cd^{2+} Ions on
597 Vermiculite. Sep. Sci. Technol. 2010;45:277-287
598 Long, H.; Wu, P.X.; Zhu, N.W. Evaluation of Cs^{+} removal from aqueous solution by
599 adsorption on ethylamine-modified montmorillonite. Chem. Eng. J.
600 2013;225:237-244
601 Lwin, C.S.; Seo, B.H.; Kim, H.U.; Owens, G.; Kim, K.R. Application of soil

602 amendments to contaminated soils for heavy metal immobilization and
603 improved soil quality—a critical review. Soil Sci. Plant Nutr. 2018;64:156-167
604 Ma, L.; Abuduwaili, J.; Li, Y.; Liu, W. Anthropogenically disturbed potentially toxic
605 elements in roadside topsoils of a suburban region of Bishkek, Central Asia.
606 Soil Use Manage. 2019;35:283-292
607 Madejova, J. FTIR techniques in clay mineral studies. Vib. Spectrosc. 2003;31:1-10
608 Manahan, S.E. Environmental chemistry.Tenth edition.. Boca Raton, FL : CRC Press;
609 2017
610 Markovic, J.; Jovic, M.; Smiciklas, I.; Sljivic-Ivanovic, M.; Onjia, A.; Trivunac, K.;
611 Popovic, A. Cadmium retention and distribution in contaminated soil: effects
612 and interactions of soil properties, contamination level, aging time and in situ
613 immobilization agents. Ecotox. Environ. Safe. 2019;174:305-314
614 MEP. National soil contamination survey report. China: Ministry of Environmental
615 Protection; 2014
616 Merrikhpour, H.; Jalali, M. Comparative and competitive adsorption of cadmium,
617 copper, nickel, and lead ions by Iranian natural zeolite. Clean Technol. Environ.
618 Policy 2013;15:303-316
619 Mittal, A.; Ahmad, R.; Hasan, I. Biosorption of Pb^{2+}, Ni^{2+} and Cu^{2+} ions from aqueous
620 solutions by L-cystein-modified montmorillonite-immobilized alginate
621 nanocomposite. Desalin. Water Treat. 2016;57:17790-17807
622 Mukhopadhyay, R.; Bhaduri, D.; Sarkar, B.; Rusmin, R.; Hou, D.; Khanam, R.; Sarkar,
623 S.; Kumar Biswas, J.; Vithanage, M.; Bhatnagar, A.; Ok, Y.S. Clay-polymer

624 nanocomposites: Progress and challenges for use in sustainable water
625 treatment. J. Hazard. Mater. 2019;383:121125
626 Ni, X.; Li, Z.; Wang, Y. Adsorption characteristics of anionic surfactant sodium
627 dodecylbenzene sulfonate on the surface of montmorillonite minerals. Front.
628 Chem. 2018;6
629 NJDEP. Technical Guidance on the Capping of Sites Undergoing Remediation. in:
630 New Jersey Department of Environmental Protection T., NJ (2014), ed; 2014
631 O'Connor, D.; Peng, T.Y.; Li, G.H.; Wang, S.X.; Duan, L.; Mulder, J.; Cornelissen, G.;
632 Cheng, Z.L.; Yang, S.M.; Hou, D.Y. Sulfur-modified rice husk biochar: A green
633 method for the remediation of mercury contaminated soil. Sci. Total Environ.
634 2018;621:819-826
635 O'Connor, D.; Zheng, X.; Hou, D.; Shen, Z.; Li, G.; Miao, G.; O'Connell, S.; Guo, M.
636 Phytoremediation: Climate change resilience and sustainability assessment at
637 a coastal brownfield redevelopment. Environment International 2019;130
638 Rizwan, M.; Ali, S.; Rehman, M.Z.U.; Rinklebe, J.; Tsang, D.C.W.; Bashir, A.; Maqbool,
639 A.; Tack, F.M.G.; Ok, Y.S. Cadmium phytoremediation potential of Brassica
640 crop species: A review. Sci. Total Environ. 2018;631-632:1175-1191
641 Rosin, P.; Rammler, E. Laws governing the fineness of powdered coal. J. Inst. Fuel
642 (UK) 1933;7:29-36
643 Rumble, J.R.; Lide, D.R.; Bruno, T.J. CRC handbook of chemistry and physics : a
644 ready-reference book of chemical and physical data.99th edition. Boca Raton :
645 CRC Press; 2018

646 Saleh, T.A.; Tuzen, M.; Sari, A. Polyamide magnetic palygorskite for the simultaneous
647 removal of Hg(II) and methyl mercury; with factorial design analysis. J. Environ.
648 Manage. 2018;211:323-333
649 Shaban, M.; Abukhadra, M.R. Geochemical evaluation and environmental application
650 of Yemeni natural zeolite as sorbent for Cd^{2+} from solution: kinetic modeling,
651 equilibrium studies, and statistical optimization. Environ. Earth Sci. 2017;76:16
652 Shen, W.G.; Cao, L.; Li, Q.; Zhang, W.S.; Wang, G.M.; Li, C.C. Quantifying CO_2
653 emissions from China's cement industry. Renew. Sust. Energ. Rev.
654 2015;50:1004-1012
655 Shen, Z.; Jin, F.; O'Connor, D.; Hou, D. Solidification/Stabilization for Soil Remediation:
656 An Old Technology with New Vitality. Environ. Sci. Technol. 2019a;
657 Shen, Z.; Pan, S.; Hou, D.; O'Connor, D.; Jin, F.; Mo, L.; Xu, D.; Zhang, Z.; Alessi, D.S.
658 Temporal effect of MgO reactivity on the stabilization of lead contaminated soil.
659 Environment international 2019b;131:104990
660 Shen, Z.T.; Fan, X.L.; Hou, D.Y.; Jin, F.; O'Connor, D.; Tsang, D.C.W.; Ok, Y.S.; Alessi,
661 D.S. Risk evaluation of biochars produced from Cd-contaminated rice straw
662 and optimization of its production for Cd removal. Chemosphere
663 2019c;233:149-156
664 Shen, Z.T.; Hou, D.Y.; Xu, W.D.; Zhang, J.Z.; Jin, F.; Zhao, B.; Pan, S.Z.; Peng, T.Y.;
665 Alessi, D.S. Assessing long-term stability of cadmium and lead in a soil
666 washing residue amended with MgO-based binders using quantitative
667 accelerated ageing. Sci. Total Environ. 2018a;643:1571-1578

668 Shen, Z.T.; Hou, D.Y.; Zhao, B.; Xu, W.D.; Ok, Y.S.; Bolan, N.S.; Alessi, D.S. Stability
669 of heavy metals in soil washing residue with and without biochar addition
670 under accelerated ageing. Sci. Total Environ. 2018b;619:185-193
671 Sheng, F.; Ling, J.Y.; Hong, R.; Jin, X.; Wang, C.; Zhong, H.; Gu, X.Y.; Gu, C. A new
672 pathway of monomethylmercury photodegradation mediated by singlet oxygen
673 on the interface of sediment soil and water. Environ. Pollut. 2019;248:667-675
674 Shi, J.; Fan, X.; Tsang, D.C.W.; Wang, F.; Shen, Z.; Hou, D.; Alessi, D.S. Removal of
675 lead by rice husk biochars produced at different temperatures and implications
676 for their environmental utilizations. Chemosphere 2019;235:825-831
677 Shirzadi, H.; Nezamzadeh-Ejhieh, A. An efficient modified zeolite for simultaneous
678 removal of Pb(II) and Hg(II) from aqueous solution. J. Mol. Liq.
679 2017;230:221-229
680 Sierra, C.; Gallego, J.R.; Afif, E.; Menendez-Aguado, J.M.; Gonzalez-Coto, F. Analysis
681 of soil washing effectiveness to remediate a brownfield polluted with pyrite
682 ashes. J. Hazard. Mater. 2010;180:602-608
683 Skoog, D.A. Principles of Instrumental Analysis.Seventh edition.. Boston : Cengage
684 Learning; 2018
685 Song, Y.A.; Kirkwood, N.; Maksimovic, C.; Zhen, X.D.; O'Connor, D.; Jin, Y.L.; Hou,
686 D.Y. Nature based solutions for contaminated land remediation and brownfield
687 redevelopment in cities: A review. Sci. Total Environ. 2019;663:568-579
688 Stefan, M.; Stefan, D.S. Study of Cadmium Sorption on Na-Montmorillonite. Rev.
689 Chim. 2009;60:1169-1174

690 Tran, H.N.; You, S.J.; Hosseini-Bandegharaei, A.; Chao, H.P. Mistakes and
691 inconsistencies regarding adsorption of contaminants from aqueous solutions:
692 A critical review. Water Res. 2017;120:88-116
693 Tran, L.; Wu, P.X.; Zhu, Y.J.; Yang, L.; Zhu, N.W. Highly enhanced adsorption for the
694 removal of Hg(II) from aqueous solution by
695 Mercaptoethylamine/Mercaptopropyltrimethoxysilane functionalized
696 vermiculites. J. Colloid Interface Sci. 2015;445:348-356
697 Unuabonah, E.I.; Olu-Owolabi, B.I.; Adebowale, K.O. Competitive adsorption of metal
698 ions onto goethite-humic acid-modified kaolinite clay. Int. J. Environ. Sci.
699 Technol. 2016;13:1043-1054
700 USEPA. Method 1311 Toxicity Characteristic Leaching Procedure. 1992;
701 USEPA. Appendix to Method 1631: Total Mercury in Tissue, Sludge, Sediment, and
702 Soil by Acid Digestion and Brcl Oxidation. 2001;
703 Wang, H.; Wang, X.J.; Li, J.; Jing, H.P.; Xia, S.Q.; Liu, F.Q.; Zhao, J.F. Comparison of
704 palygorskite and struvite supported palygorskite derived from phosphate
705 recovery in wastewater for in-situ immobilization of Cu, Pb and Cd in
706 contaminated soil. J. Hazard. Mater. 2018a;346:273-284
707 Wang, J.X.; Feng, X.B.; Anderson, C.W.N.; Xing, Y.; Shang, L.H. Remediation of
708 mercury contaminated sites - A review. J. Hazard. Mater. 2012;221:1-18
709 Wang, L.; Cho, D.W.; Tsang, D.C.W.; Cao, X.D.; Hou, D.Y.; Shen, Z.T.; Alessi, D.S.;
710 Ok, Y.S.; Poon, C.S. Green remediation of As and Pb contaminated soil using
711 cement-free clay-based stabilization/solidification. Environ. Int.

712 2019a;126:336-345
713 Wang, L.; Yu, K.Q.; Li, J.S.; Tsang, D.C.W.; Poon, C.S.; Yoo, J.C.; Baek, K.; Ding,
714 S.M.; Hou, D.Y.; Dai, J.G. Low-carbon and low-alkalinity
715 stabilization/solidification of high-Pb contaminated soil. Chem. Eng. J.
716 2018b;351:418-427
717 Wang, Y.; O'Connor, D.; Shen, Z.; Lo, I.M.C.; Tsang, D.C.W.; Pehkonen, S.; Pu, S.;
718 Hou, D. Green synthesis of nanoparticles for the remediation of contaminated
719 waters and soils: Constituents, synthesizing methods, and influencing factors.
720 J. Clean. Prod. 2019b;226:540-549
721 Weller, M. Inorganic chemistry.7th edition.. Oxford : Oxford University Press; 2018
722 WHO. Ten chemicals of major health concern. World Health Organization 2017;
723 Wu, P.X.; Wu, W.M.; Li, S.Z.; Xing, N.; Zhu, N.W.; Li, P.; Wu, J.H.; Yang, C.; Dang, Z.
724 Removal of Cd^{2+} from aqueous solution by adsorption using
725 Fe-montmorillonite. J. Hazard. Mater. 2009;169:824-830
726 Wu, P.X.; Zhang, Q.; Dai, Y.P.; Zhu, N.W.; Dang, Z.; Li, P.; Wu, J.H.; Wang, X.D.
727 Adsorption of Cu(II), Cd(II) and Cr(III) ions from aqueous solutions on humic
728 acid modified Ca-montmorillonite. Geoderma 2011;164:215-219
729 Wu, Y.J.; Zhou, H.; Zou, Z.J.; Zhu, W.; Yang, W.T.; Peng, P.Q.; Zeng, M.; Liao, B.H. A
730 three-year in-situ study on the persistence of a combined amendment
731 (limestone+sepiolite) for remedying paddy soil polluted with heavy metals.
732 Ecotox. Environ. Safe. 2016;130:163-170
733 Xia, Y.; Liu, H.; Guo, Y.; Liu, Z.; Jiao, W. Immobilization of heavy metals in

contaminated soils by modified hydrochar: Efficiency, risk assessment and potential mechanisms. Sci. Total Environ. 2019;685:1201-1208

Xu, Y.; Liang, X.F.; Xu, Y.M.; Qin, X.; Huang, Q.Q.; Wang, L.; Sun, Y.B. Remediation of Heavy Metal-Polluted Agricultural Soils Using Clay Minerals: A Review. Pedosphere 2017;27:193-204

Yang, J.; Yu, K.; Liu, C. Chromium immobilization in soil using quaternary ammonium cations modified montmorillonite: Characterization and mechanism. J. Hazard. Mater. 2017;321:73-80

Zauro, S.A.; Vishalakshi, B. Pectin graft copolymer-montmorillonite composite: Synthesis, swelling and divalent metal ion adsorption. Sep. Sci. Technol. 2018;53:2170-2185

Zhang, P.; O'Connor, D.; Wang, Y.; Jiang, L.; Xia, T.; Wang, L.; Tsang, D.C.W.; Ok, Y.S.; Hou, D. A green biochar/iron oxide composite for methylene blue removal. J. Hazard. Mater. 2020;384

Zhang, Y.H.; Hou, D.Y.; O'Connor, D.; Shen, Z.T.; Shi, P.L.; Ok, Y.S.; Tsang, D.C.W.; Wen, Y.; Luo, M.N. Lead contamination in Chinese surface soils: Source identification, spatial-temporal distribution and associated health risks. Crit. Rev. Environ. Sci. Technol. 2019;49:1386-1423

Zolotoyabko, E. Basic concepts of X-ray diffraction. Weinheim, Germany : Wiley-VCH Verlag GmbH & Co. KGaA; 2014

Highlights

- A novel clay-based Cd and Hg stabilization approach was proposed.
- FESEM/EDS, BET, FTIR, XRD results reveal the characteristics of HA-Mont.
- Quantitative accelerated ageing was adopted to examine the long-term stability.
- Ageing features of immobilization processes were depicted by a Weibull model.

***Graphical Abstract**